International Journal of Heat and Mass Transfer 54 (2011) 4349–4359

Contents lists available at ScienceDirect

International Journal of Heat and Mass Transfer

journal homepage: www.elsevier.com/locate/ijhmt

Heat conduction in nanofluids: Structure–property correlation

Jing Fan, Liqiu Wang *

Department of Mechanical Engineering, The University of Hong Kong, Pokfulam Road, Hong Kong

ARTICLE INFO

Article history:
Received 30 April 2010
Received in revised form 30 April 2011
Available online 3 June 2011

Keywords:
Nanofluids
Heat conduction
Effective thermal conductivity
Phase lags
Microstructure

ABSTRACT

We examine numerically the effects of particle-fluid thermal conductivity ratio, particle volume fraction, and particle morphology on nanofluids effective thermal conductivity and phase lags of heat flux and temperature gradient, for six types of nanofluids containing sphere, cube, hollow sphere, hollow cube, slab-cross and column-cross nanoparticles, respectively. The particle's radius of gyration and the non-dimensional particle-fluid interfacial area are found to be two characteristic parameters for the effect of particles' geometrical structure on the effective thermal conductivity. The nanoparticles with larger values of these two parameters can change fluid conductivity more significantly. Due to the enhanced particle-fluid interfacial heat transfer, the nanofluid effective thermal conductivity can practically reach the Hashin–Shtrikman bounds when the particle-phase connects to form a network and separates the base fluid into a dispersed phase. The particle aggregation can effectively affect the effective thermal conductivity when the separation distance among particles is smaller than about one fifth of the particles' dimension. For the nanofluids considered in the present work, the phase lags of heat flux and temperature gradient scale with the square of particle dimension and range from 10^{-11} s to 10^{-7} s; the effect of cross-coupling between the heat conduction in the fluid and particle phases is weak; the phase lag of temperature gradient is larger than that of heat flux such that the heat conduction in them is diffusion-dominant and their effective thermal conductivity can be well predicted by the predictive models developed in the present work based on the classical diffusion theory for two-phase systems.

1. Introduction

Nanofluids, fluid suspensions of nanometer-sized structures, have recently been demonstrated to have thermal conductivities far superior to that of the fluid alone [1–4]. This and their other distinctive features offer unprecedented potential for many applications in various fields including energy, bio- and pharmaceutical industry, and chemical, electronic, environmental, material, medical and thermal engineering [1–4].

In an attempt to identify effects of microscale physics on thermal conductivity, a relatively intensified effort has been made on determining thermal conductivity of nanofluids from experiments, particularly for nanofluids with spherical nanoparticles or nanotubes. While the data from these experiments have enabled some trends to be identified, there is still no consensus on the effects of some parameters such as particle size, shape, distribution and additives in the nanofluids [1–5]. Wide discrepancies and inconsistencies also exist in the reported conductivity data due to a limited understanding of the precise nature of heat conduction in nanofluids, the poor microstructure characterization and the unavailability of nanofluids with various microstructures [1–5]. In many cases the microstructural parameters were not measured by the experimenters themselves but rather taken from the powder manufacturers' nominal information.

Suggested reasons for the experimental finding of significant conductivity enhancement include nanoparticles' Brownian motion [6–8], liquid layering at the liquid-particle interface [9,10], particle-phase morphology [11–19] and coupled (cross) transport [19–21]. Here, the effect of particle morphology contains those from the particle shape, connectivity among particles (including and generalizing the nanoparticle clustering/aggregating in the literature), and particles' distribution in nanofluids. The critical assessment of these contributions signifies the importance of particle morphology and coupled transport in determining nanofluid heat conduction and thermal conductivity [19,22,23]. While the direct contributions of ordered liquid layer and particles' Brownian motion to the nanofluid conductivity is negligible, their indirect effects can be significant via their influence on the particle-phase morphology and/or the coupled transport [19].

In a nanofluid system, there are normally two or more transport processes that occur simultaneously. The cross coupling among these processes causes new induced flows occurring without or against its primary thermodynamic driving force and is capable of changing the nature of heat conduction via inducing thermal waves and resonance of various orders [19–21]. Depending on the

* Corresponding author.
E-mail address: lqwang@hku.hk (L. Wang).

0017-9310/$ - see front matter © 2011 Elsevier Ltd. All rights reserved.
doi:10.1016/j.ijheatmasstransfer.2011.05.009

Nomenclature

A_{fp}	particle-fluid interface area inside the unit cell
a	side length of the cube
a_c	side length of the square column of the column-cross particle
a_i	inner side length of the hollow cube
a_o	outer side length of the hollow cube
a_s	slab side length of the slab-cross particle
a_v	interfacial area per unit volume
b_l	closure variable
c_p	specific heat
d_p	diameter of the sphere particle
h	interfacial heat transfer coefficient
IA	non-dimensional interfacial area in the unit cell
k	thermal conductivity
k_e	effective thermal conductivity
k_{ff}, k_{fp}, k_{pf}, k_{pp}	macroscale effective thermal conductivity coefficients
L_A	distance between each particle and the center plane of the unit cell containing eight sphere particles
l_c	column length of the column-cross particle
l_u	dimension of the unit cell
n	a parameter depending on particle morphology and k_p/k_f in Eq. (29)
$\mathbf{n}_{fp}$	utwardly-directed unit normal vector pointing from the base fluid to the particle
R_g	radius of gyration
r	radius of the sphere
r_i	inner radius of the hollow sphere
r_o	outer radius of the hollow sphere
S	closure variable
V_f	fluid volume inside the unit cell
V_p	particle volume inside the unit cell
w_s	slab thickness of the slab-cross particle
X	a parameter depending on particle morphology and k_p/k_f in Eq. (28)
φ	particle volume fraction
ρ	density
τ_q	phase lag of heat flux
τ_T	phase lag of temperature gradient

Subscripts

f	base fluid phase
p	particle phase

microscale physics (factors like material properties of nanoparticles and base fluid, nanoparticles' morphology in the base fluid, and interfacial properties and dynamic processes on particle-fluid interfaces), the heat diffusion and thermal waves may either enhance or counteract each other. It is thus important to quantify when and to what extent thermal waves become important.

The particle-phase morphology in nanofluids can vary from a well-dispersed configuration in base fluids to an interconnected configuration as a continuous phase. Such a morphology variation will change nanofluid effective thermal conductivity significantly [24], a phenomenon credited to the particle clustering/aggregation in the literature. Although nanofluid thermal conductivity depends heavily on the morphology of nanoparticles, its lower and upper bounds can be completely determined by the volume fractions and conductivities of the two phases. Without considering the effect of interfacial resistance and cross coupling among various transport processes, these bounds have been well developed based on the classical effective-medium theory and termed as the Hashin–Shtrikman (H–S) bounds [25]. However, the microscopic mechanism responsible for these bounds has been left unaddressed. Furthermore, the theory of H–S bounds has not offered the answers to questions regarding parameters that characterize the effects of particles' geometrical structures and contributions of the two phases to the effective conductivity.

The present work attempts to address these key issues based on the first-principle model of heat conduction in nanofluids with cross-coupling between the heat conduction in the fluid and particle phases being considered [20,21,26]. Especially, we address these issues numerically for six types of nanofluids containing in-line arrays of spheres, squares, hollow spheres, hollow squares, column-cross particles and slab-cross particles, respectively [Fig. 1(a)–(f)]. While the theoretical model and numerical scheme are the three-dimensional (3D) extension of two-dimensional (2D) version used in [24], the present work employs different particle shapes to examine the dependency of effective thermal conductivity on the particles' morphology and to identify the characteristic parameters for the effect of particles' morphology in practical 3D nanofluids. The present work also addresses the following key issues that have not been addressed in [24]: (i) contributions of the base fluid, particles, and cross-coupling heat conduction between the fluid and particle phases to nanofluid effective thermal conductivity, (ii) microscopic mechanism responsible for H–S bounds, (iii) phase lags of temperature gradient and heat flux, and (iv) predictive models of effective thermal conductivity for six types of 3D nanofluids.

2. Governing equations and numerical algorithm

We consider six types of nanofluids containing in-line arrays of spheres, cubes, hollow spheres, hollow cubes, slab-cross particles (consisting of three mutually perpendicular square slabs), and column-cross particles (consisting of three mutually perpendicular square columns), respectively, thus their microstructures can be represented by the unit cells in Fig. 1(a)–(f). In Fig. 1, l_u denotes the dimensions of the unit-cell in all x-, y- and z-directions.

For these nanofluids, their effective thermal conductivity k_e, phase lag of heat flux τ_q and phase lag of temperature gradient τ_T are [20]:

$$k_e = k_{ff} + k_{fp} + k_{pf} + k_{pp}, \tag{1}$$

$$\tau_q = \frac{\gamma_f \gamma_p}{h a_v (\gamma_f + \gamma_p)}, \tag{2}$$

$$\tau_T = \frac{\gamma_f k_{pp} + \gamma_p k_{ff}}{h a_v k_e}, \tag{3}$$

where

$$k_{ff} = (1-\varphi)k_f + \int_{A_{fp}} \mathbf{n}_{fp} k_f b_l \, dA, \tag{4}$$

$$k_{fp} = k_{pf} = -\int_{A_{fp}} \mathbf{n}_{fp} k_p b_l \, dA, \tag{5}$$

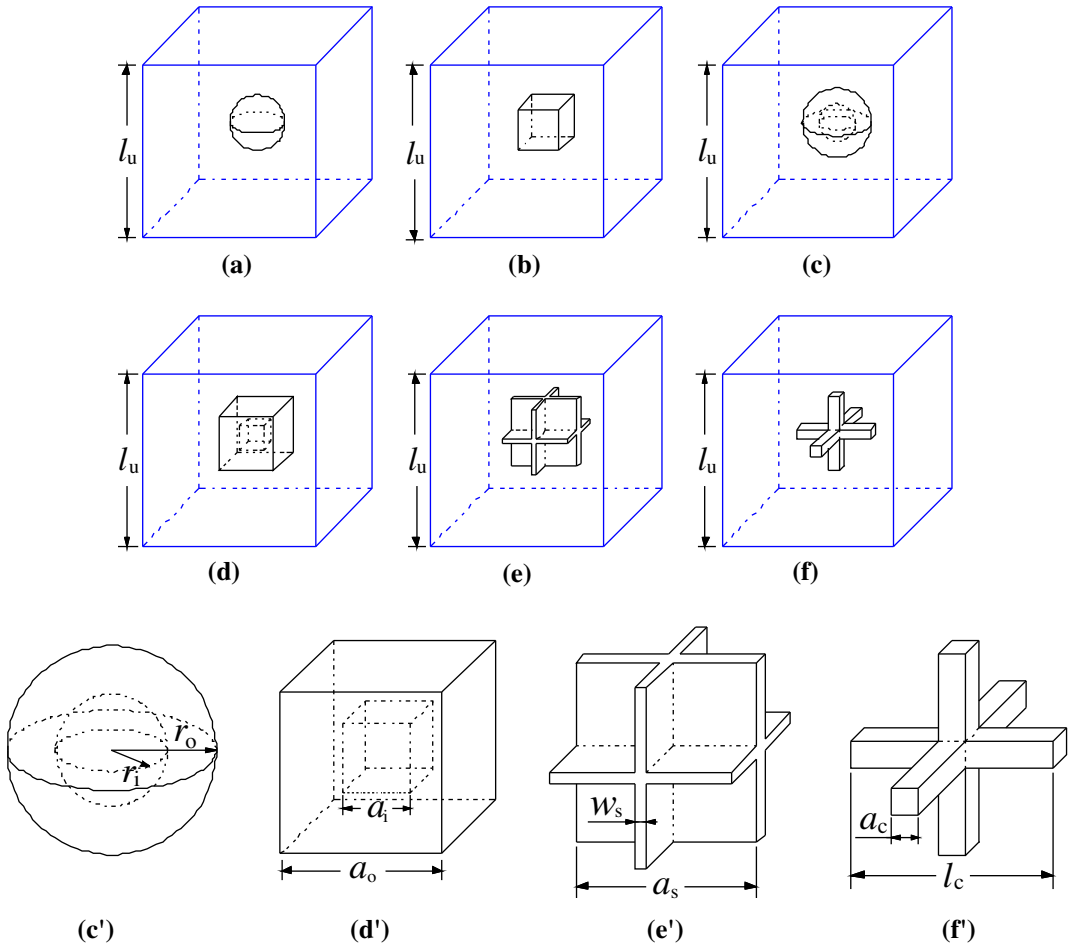

Fig. 1. Unit cells for nanofluids containing in-line arrays of spheres (a), cubes (b), hollow spheres (c), hollow cubes (d), slab-cross particles (e), and column-cross particles (f); the enlarged sketches for the last four particles with geometrical parameters marked in (c′)–(f′).

$$k_{pp} = \varphi k_p + \frac{k_p}{k_f}\int_{A_{fp}} \mathbf{n}_{fp} k_p b_l \, dA, \tag{6}$$

$$ha_v = \frac{\varphi}{\int_{V_p} S dV}, \tag{7}$$

$$\gamma_f = (1-\varphi)(\rho c_p)_f, \quad \gamma_p = \varphi(\rho c_p)_p. \tag{8}$$

Heat conduction is diffusion dominant when $\tau_T/\tau_q > 1$ and thermal-wave dominant when $\tau_T/\tau_q < 1$ [20,21]. In Eqs. (1)–(8), subscripts f and p denote fluid- and particle-phases, respectively. φ is the particle volume fraction. k_f and k_p are the thermal conductivities of the base fluid and the particles, respectively. $\mathbf{n}_{fp}$ is the outwardly-directed unit normal vector pointing from the base fluid to the particle. ρ and c_p are the density and specific heat, respectively. A_{fp} and V_p are the particle-fluid interface area and the particle volume inside the unit cell respectively. k_{ff} and k_{pp} are effective thermal conductivity coefficients representing the contribution of fluid and particle phases respectively to the effective thermal conductivity. k_{fp} and k_{pf} are cross-coupling thermal conductivity coefficients that come from, and thus characterize the importance of, the cross-coupling between heat conduction in the fluid and particles; and $k_{fp} = k_{pf}$ [27]. All these four coefficients depend on the distribution of b_l, which is a closure variable that links microscale and macroscale through the following closure problem I [20,27].

ha_v is the volumetric particle-fluid interfacial heat transfer coefficient, with a_v being the interfacial area per unit volume. The value of ha_v depends on the closure variable S which also links microscale and macroscale and satisfies the closure problem II [20,27].

2.1. Problem I

$$\nabla\cdot(k\nabla b_l) = -\nabla\cdot(\phi_f k) \tag{9a}$$

$$b_l(x+l_u) = b_l(x), \quad b_l(y+l_u) = b_l(y), \quad b_l(z+l_u) = b_l(z) \tag{9b}$$

$$\int_{V_f} b_l \, dV = 0, \int_{V_p} b_l \, dV = 0 \tag{9c}$$

2.2. Problem II

$$\nabla\cdot(k\nabla S) = -\left(\frac{\phi_p}{\varphi} - \frac{\phi_f}{1-\varphi}\right) \tag{10a}$$

$$S(x+l_u) = S(x), \quad S(y+l_u) = S(y), \quad S(z+l_u) = S(z) \tag{10b}$$

$$\int_{V_f} S dV = 0, \quad ha_v \int_{V_p} S dV = \varphi \tag{10c}$$

where V_f stands for the fluid volume inside the unit cell; ϕ_f, ϕ_p and k are defined by

$$\phi_f = \begin{cases} 1, & \text{in } V_f \\ 0, & \text{in } V_p \end{cases}, \quad \phi_p = \begin{cases} 0, & \text{in } V_f \\ 1, & \text{in } V_p \end{cases}, \quad k = \begin{cases} k_f, & \text{in } V_f \\ k_p, & \text{in } V_p \end{cases} \tag{11}$$

For the nanofluids considered in the present work, their unit cells are symmetric with respect to all three coordinates x, y and z. By using the periodic boundary conditions [Eqs. 9(b) and 10(b)], we can readily obtain that

$$b_I\left(-\frac{l_u}{2}, y, z\right) = 0, \quad b_I\left(\frac{l_u}{2}, y, z\right) = 0 \tag{12a}$$

$$\frac{\partial b_I}{\partial y}\left(x, -\frac{l_u}{2}, z\right) = 0, \quad \frac{\partial b_I}{\partial y}\left(x, \frac{l_u}{2}, z\right) = 0 \tag{12b}$$

$$\frac{\partial b_I}{\partial z}\left(x, y, -\frac{l_u}{2}\right) = 0, \quad \frac{\partial b_I}{\partial z}\left(x, y, \frac{l_u}{2}\right) = 0 \tag{12c}$$

$$\frac{\partial S}{\partial x}\left(-\frac{l_u}{2}, y, z\right) = 0, \quad \frac{\partial S}{\partial x}\left(\frac{l_u}{2}, y, z\right) = 0 \tag{12d}$$

$$\frac{\partial S}{\partial y}\left(x, -\frac{l_u}{2}, z\right) = 0, \quad \frac{\partial S}{\partial y}\left(x, \frac{l_u}{2}, z\right) = 0 \tag{12e}$$

$$\frac{\partial S}{\partial z}\left(x, y, -\frac{l_u}{2}\right) = 0, \quad \frac{\partial S}{\partial z}\left(x, y, \frac{l_u}{2}\right) = 0 \tag{12f}$$

Since the solutions of Problems I and II are unique, we can replace the periodic boundary conditions [Eqs. (9b) and (10b)] by Eqs. (12a)–(12f) without changing their final solutions.

Problems I and II with boundary conditions (12a)–(12f) are solved numerically. The numerical scheme, based on the finite volume method, is an adaptation of that in [28,29]. The main features of this method include a central difference scheme for the diffusion terms and an equation-solving scheme consisting of an alternating-direction line-by-line iterative procedure (ADI) with block-correction technique.

The non-uniform structural grid is used for the whole unit cell, making the particle-fluid interface covered with finer grid. We check the variation of computational results by reducing the grid size into a half until the variation is less than 1% so that the results are considered to be grid-size independent. The solution is assumed to be convergent in a numerical sense if the maximum relative error of the computed variables over the whole unit cell is less than 10^{-8} between successive iterations.

The initial calculation for nanofluid containing suspended spheres [Fig. 1(a)] with $\varphi = 0.01, 0.03$ and 0.05 is performed to verify the code and the accuracy. In Fig. 2(d), the variation of k_e/k_f (ratio between the nanofluid effective thermal conductivity and the base-fluid conductivity) with k_p/k_f is compared with the prediction of Maxwell–Garnett formula [30],

$$\frac{k_e}{k_f} = 1 + \frac{3\varphi(k_p/k_f - 1)}{k_p/k_f + 2 - \varphi(k_p/k_f - 1)} \tag{13}$$

showing an excellent agreement.

3. Results and discussion

3.1. Contributions of base fluid, particles and cross-coupling, and particle-fluid interfacial energy transport

k_{ff}, k_{pp} and $2k_{fp}$ represent the contributions of base fluid, particles, and cross-coupling between the heat conduction in the fluid and particle phases respectively, to the effective thermal conductivity k_e. ha_v characterizes the strength of particle-fluid interfacial energy transport. Fig. 2(a)–(e) illustrates variations of k_{ff}/k_f, k_{fp}/k_f, k_{pp}/k_f, k_e/k_f (normalized by the base-fluid conductivity k_f), and interfacial heat transfer coefficient $ha_v l_u^2/k_f$ (normalized by k_f/l_u^2) with particle-fluid conductivity ratio k_p/k_f, particle volume fraction φ and particle morphology for nanofluids in Fig. 1(a)–(d). The inner radius (r_i) and inner side length (a_i) of the hollow sphere and hollow cube are taken as a half of their respective outer counterparts (r_o) and (a_o).

The variations of k_{ff}/k_f, k_{fp}/k_f, and k_{pp}/k_f have some similar features with those in two-dimensional cases: all increase with particle-fluid thermal conductivity ratio k_p/k_f; their sensitivity to the particle shape is stronger at larger particle volume fraction; the k_{ff}/k_f approaches to the limit value $(1-\varphi)$ as k_p/k_f increases to infinity; k_{ff}/k_f (k_{pp}/k_f) is nearly independent of the particle shape when k_p/k_f is larger (smaller) than 1. Since the particles can be well regarded as the dispersed phase, the coefficient k_{fp}/k_f is not sensitive to particle shape either, and towards to the limit value $\varphi(0)$ as k_p/k_f increases to infinity (decreases to 0). As the particle-fluid conductivity ratio k_p/k_f increases from 0 to infinity, k_e/k_f increases from a lower limit to a higher limit, both of which depend on the particle shape and volume fraction [Fig. 2(d)]. When the particle-fluid conductivity ratio k_p/k_f is either sufficiently large or sufficiently small such that the particle can be regarded as either isothermal or adiabatic, therefore, the nanoparticle's conductivity has a negligible effect on the effective thermal conductivity. This phenomenon is also consistent with the two-dimensional cases under small radius of gyration and particle-fluid interfacial area in a unit cell [31].

In 3D nanofluids, the particle shape with lower values of k_{ff}/k_f at $k_p/k_f < 1$ does not necessarily lead to higher values of k_{pp}/k_f at $k_p/k_f > 1$ at certain particle volume fraction φ, [the cube and hollow-sphere particles in Fig. 2(a) and (c)]. This differs from that in 2D nanofluids [24,31]. The cube nanofluid has thus a higher effective thermal conductivity ratio k_e/k_f than the hollow-sphere nanofluid for both $k_p/k_f < 1$ and $k_p/k_f > 1$ [Fig. 2(d)]. Moreover, the sensitivities of k_e/k_f to the particle shape, k_p/k_f and φ are obviously stronger at $k_p/k_f > 1$ than $k_p/k_f < 1$. This phenomenon also differs from that in 2D nanofluids in which particles can be well treated as the dispersed phase [24,31].

The $ha_v l_u^2/k_f$ increases with k_p/k_f and φ for all four types of nanofluids as shown in Fig. 2(e). A different feature from 2D nanofluids is the intersection of the cube-line and the hollow-sphere-line for certain particle volume fraction. It is interesting to note that a particle shape with a higher value of $ha_v l_u^2/k_f$ always leads to a higher (lower) k_e/k_f when $k_p/k_f > 1$ ($k_p/k_f < 1$). Therefore, a stronger fluid-particle interfacial heat transfer is the key to upgrade nanofluid thermal conductivity.

3.2. Parameters for characterizing effects of 3D geometrical structures of particles

The 2D simulation suggested two parameters for characterizing particle geometrical effect on nanofluid thermal conductivity [24]: the radius of gyration R_g and the non-dimensional particle-fluid interfacial area IA in the unit cell. The former is defined as the root mean square distance of each point of the particle from its centroidal axis, and thus characterizes the overall spread of the particle. The latter is the particle-fluid interfacial area in the unit cell with all lengths normalized by the unit cell dimension l_u. For fixed particle volume fraction, IA depends only on the particle shape and could thus serve as a candidate of characterizing particle geometrical effect. Table 1 lists R_g and IA as functions of the non-dimensional particle geometrical parameters for the six types of nanoparticles in Fig. 1(a)–(f). For nanoparticles in Fig. 1(a)–(d), the respective geometrical parameters are the radius r of sphere, the side length a of cube, the inner and outer radiuses r_i and r_o,

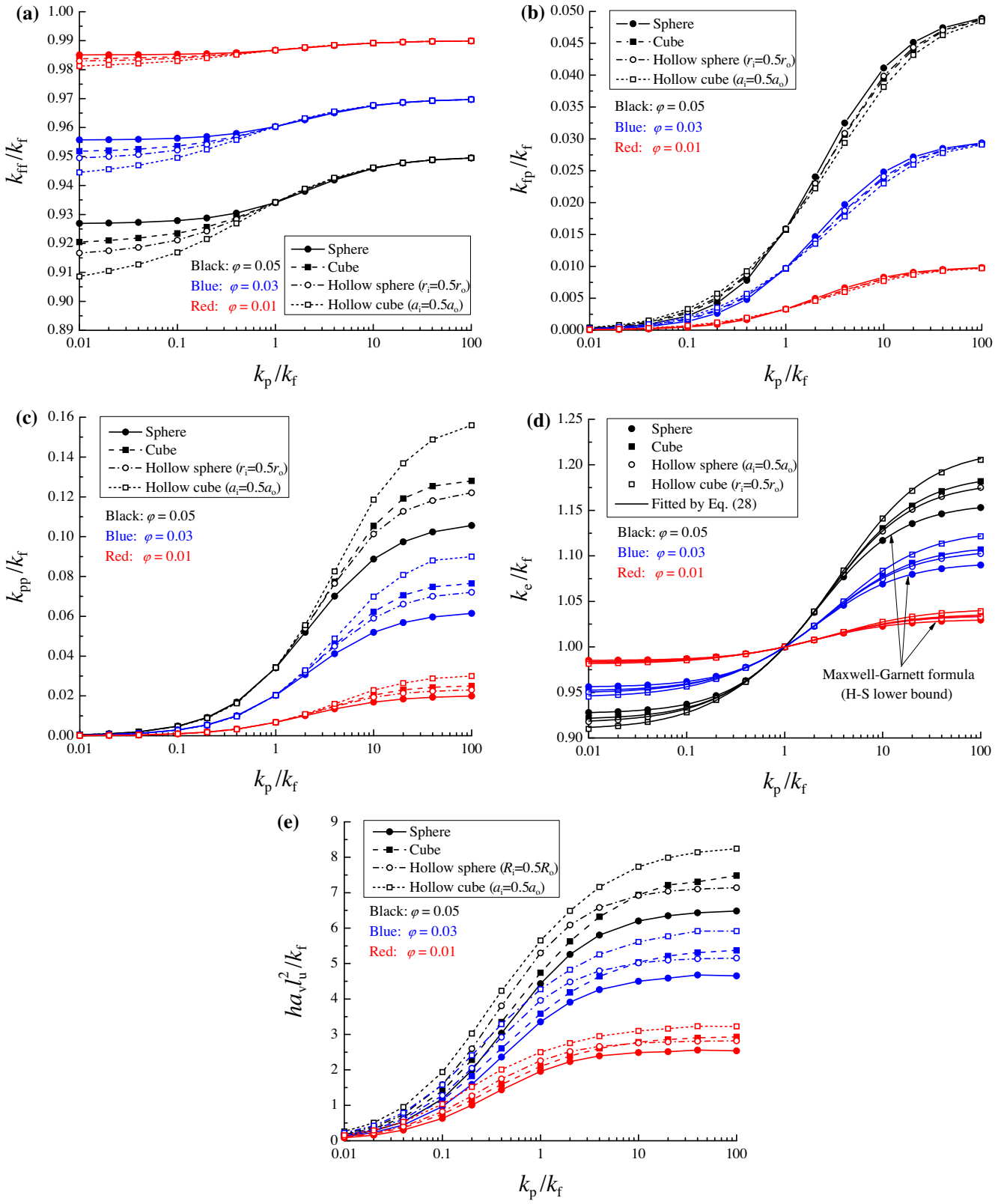

Fig. 2. Variations of k_{ff}/k_f (a), k_{fp}/k_f (b), k_{pp}/k_f (c), k_e/k_f (d), and interfacial heat transfer coefficient $ha_v l_u^2/k_f$ (e) with particle-fluid conductivity ratio k_p/k_f, particle volume fraction φ and particle morphology.

and the inner and outer side lengths a_i and a_o. For the slab-cross particle in Fig. 1(e), the geometrical parameters include the slab thickness w_s and the side length a_s of the square slab (Fig. 1 (e′)). For the column-cross particle in Fig. 1(f), the geometrical parameters contain the side length a_c of the square column and the column length l_c (Fig. 1 (f′)).

Table 1
Particle volume fraction φ, radius of gyration R_g and non-dimensional particle-fluid interfacial area IA for nanofluids in Fig. 1(a)-(f) ($\bar{\chi} = \chi/l_u$).

Nanofluids	Volume fraction φ	Radius of gyration R_g	Non-dimesnional particle-fluid interfacial area IA
Fig. 1(a)	$\frac{4}{3}\pi\bar{r}^3$	$\sqrt{\frac{2}{5}}\bar{r}$	$4\pi\bar{r}^2$
Fig. 1(b)	$\bar{a}^3$	$\frac{1}{\sqrt{6}}\bar{a}$	$6\bar{a}^2$
Fig. 1(c)	$\frac{4\pi}{3}(\bar{r}_o^3 - \bar{r}_i^3)$	$\sqrt{\frac{2}{5}(\bar{r}_o^5 - \bar{r}_i^5)/(\bar{r}_o^3 - \bar{r}_i^3)}$	$4\pi(\bar{r}_o^2 + \bar{r}_i^2)$
Fig. 1(d)	$\bar{a}_o^3 - \bar{a}_i^3$	$\sqrt{\frac{1}{6}\bar{a}_o^2 + \frac{1}{22}\bar{a}_i^2}$	$6(\bar{a}_o^2 + \bar{a}_i^2)$
Fig. 1(e)	$3\bar{w}_s\bar{a}_s^2 - 3\bar{w}_s^2\bar{a}_s + \bar{w}_s^3$	$\frac{1}{3\sqrt{2}}\sqrt{\bar{w}_s^2 + 2\bar{a}_s^2}$	$6\bar{a}_s^2$
Fig. 1(f)	$3\bar{w}_c^2\bar{l}_c - 2\bar{w}_c^3$	$\frac{1}{6}\sqrt{4\bar{w}_c^2 + 2\bar{l}_c^2}$	$12\bar{w}_c\bar{l}_c - 6\bar{w}_c^2$

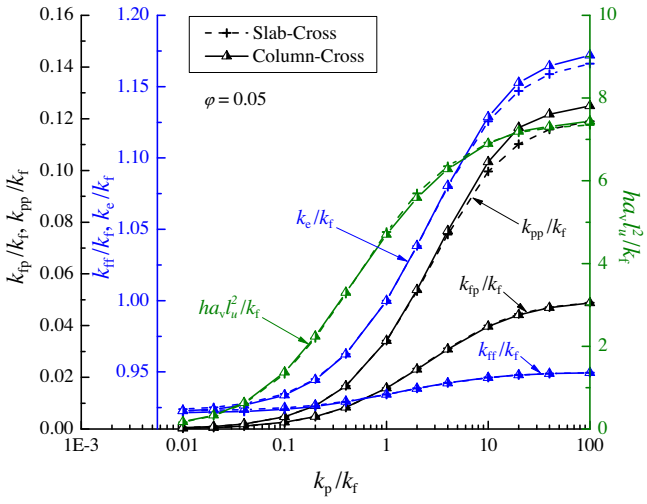

Fig. 3. k_{ff}/k_f, k_{fp}/k_f, k_{pp}/k_f, k_e/k_f, and $ha_v l_u^2/k_f$ for two nanofluids with the same non-dimensional particle-fluid interfacial area and the same radius of gyration at $\varphi = 0.05$.

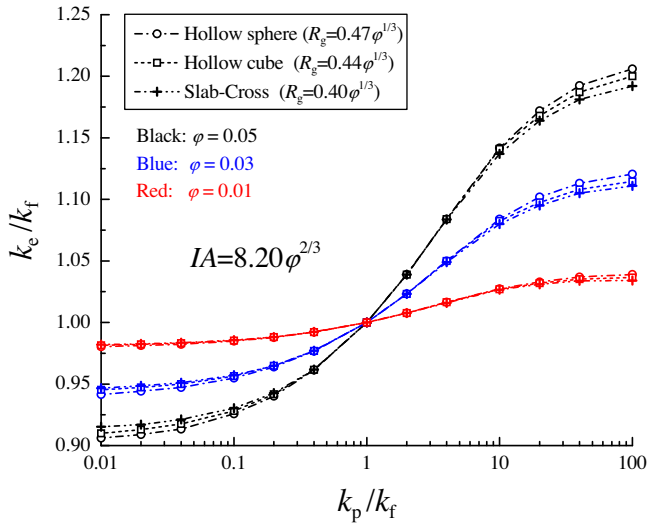

Fig. 4. Effective thermal conductivity ratio k_e/k_f as a function of k_p/k_f and φ for three nanofluids with the same non-dimensional particle-fluid interfacial area ($IA = 8.20\varphi^{2/3}$).

To address whether R_g and IA are still the characterizing parameters in 3D nanofluids, we examine k_{ff}/k_f, k_{fp}/k_f, k_{pp}/k_f, $ha_v l_u^2/k_f$ and k_e/k_f in Fig. 3 for nanofluids containing the slab-cross and column-cross particles [Fig. 1(e) and (f)] at $\varphi = 0.05$. For the same radius of gyration and non-dimensional interfacial area for both cases, particle dimensions are fixed by

$$\frac{\sqrt{\bar{w}_s^2 + 2\bar{a}_s^2}}{3\sqrt{2}} = \frac{\sqrt{4\bar{a}_c^2 + 2\bar{l}_c^2}}{6} \quad (\text{same } R_g) \tag{14}$$

$$6(\bar{a}_s - \bar{w}_s)^2 = 12\bar{a}_c(\bar{l}_c - \bar{a}_c) \quad (\text{same } IA) \tag{15}$$

$$3\bar{w}_s\bar{a}_s^2 - 3\bar{w}_s^2\bar{a}_s + \bar{w}_s^3 = 0.05 \quad (\varphi = 0.05) \tag{16}$$

$$3\bar{a}_c^2\bar{l}_c - 2\bar{a}_c^3 = 0.05 \quad (\varphi = 0.05) \tag{17}$$

Fig. 3 clearly shows that k_{ff}/k_f, k_{fp}/k_f, k_{pp}/k_f, $ha_v l_u^2/k_f$ and k_e/k_f are almost the same for two particles. Therefore, the radius of gyration and non-dimensional interfacial area are two very important parameters to characterize the effects of particles' geometrical structures.

Fig. 4 plots the variation of k_e/k_f for three types of nanofluids [Fig. 1(c)–(e)], with the same IA (at the same particle volume fraction) but different R_g, showing that k_e/k_f increases with R_g when $k_p/k_f > 1$, but decreases when $k_p/k_f < 1$. The IA-effect on k_e/k_f is shown in Fig. 5 at the same R_g (at the same particle volume fraction) for the three types of nanofluids [Fig. 1(c)–(e)]. An upgrade

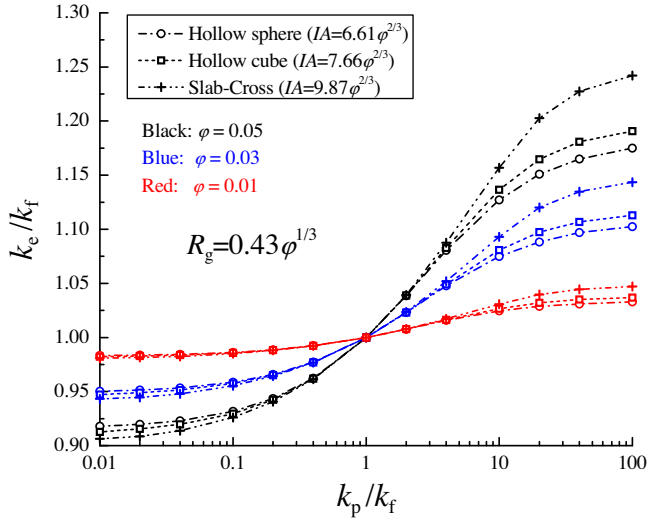

Fig. 5. Effective thermal conductivity ratio k_e/k_f as a function of k_p/k_f and φ for three nanofluids with the same radius of gyration ($R_g = 0.43\varphi^{1/3}$).

of particle IA-value will boast k_e/k_f when $k_p/k_f > 1$ and decrease k_e/k_f when $k_p/k_f < 1$. Therefore, larger values of these two parameters have stronger impacts on the conductivity change in nanofluids, a phenomenon also found for 2D nanofluids [24].

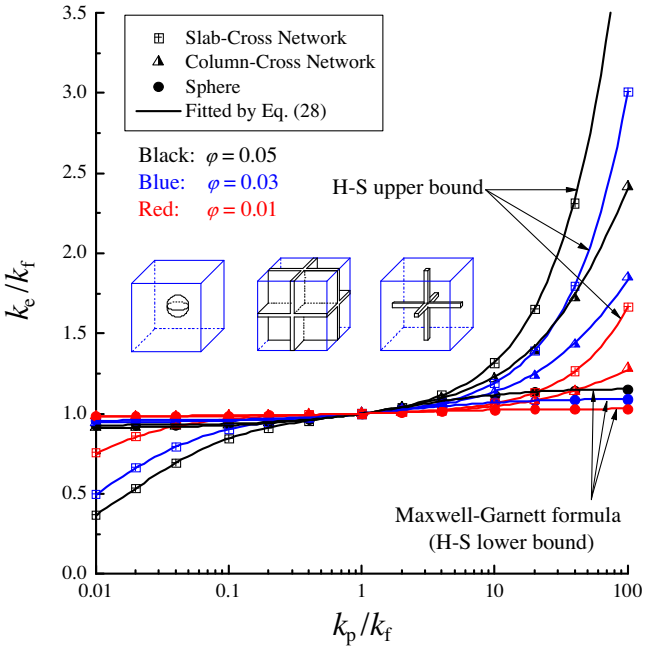

Fig. 6. Effective thermal conductivity k_e/k_f as a function of particle-aggregation morphology, k_p/k_f and φ.

3.3. Nanofluids with Hashin–Shtrikman conductivity bounds

For macroscopically homogeneous and isotropic two-phase systems such as nanofluids considered in the present work, k_e/k_f is bounded by the Hashin–Shtrikman bounds [25]:

$$k_e/k_f = k_p/k_f\left[1 - \frac{3(1-\varphi)(k_p/k_f - 1)}{3k_p/k_f - \varphi(k_p/k_f - 1)}\right] \quad (18)$$

which gives the upper bound when $k_p/k_f > 1$ and the lower bound when $k_p/k_f < 1$.

For slab-cross nanofluids in Fig. 1(e), the particles will form a connected slab-cross network in nanofluids when $a_s = l_u$ (inset in Fig. 6). Similarly, the column-cross nanoparticles in Fig. 1(f) will also form a connected network when $l_c = l_u$ (inset in Fig. 6). While the particles are connected to form a network in both cases, there is a significant difference between the two. In the former, the base fluid is separated by the particle network such that it can be regarded as a dispersed phase. In the latter, the connected particle network does not separate the base fluid into different parts such that the base fluid is still connected and cannot be reviewed as a dispersed phase.

Fig. 6 shows the variations of the effective thermal conductivity ratio k_e/k_f for three types of nanofluids containing slab-cross network, column-cross network and spheres, respectively. For the same k_p/k_f and φ, the effective thermal conductivity for the nanofluids with the connected slab-cross network is much higher than the other two nanofluids when $k_p/k_f > 1$, and much lower when $k_p/k_f < 1$. In particular, their conductivity can practically reach the Hashin–Shtrikman bounds.

When k_p/k_f is larger than 1, the effective thermal conductivity of the nanofluids containing column-cross network is much higher than that of the sphere nanofluids, but there is still some distance from the Hashin–Shtrikman bound. When k_p/k_f is smaller than 1, however, the effective thermal conductivity of the column-cross nanofluids is only slightly smaller than that of the sphere nanofluids. Unlike the sphere nanofluids, nanofluids containing slab-cross or column-cross networks do not show any level-off of

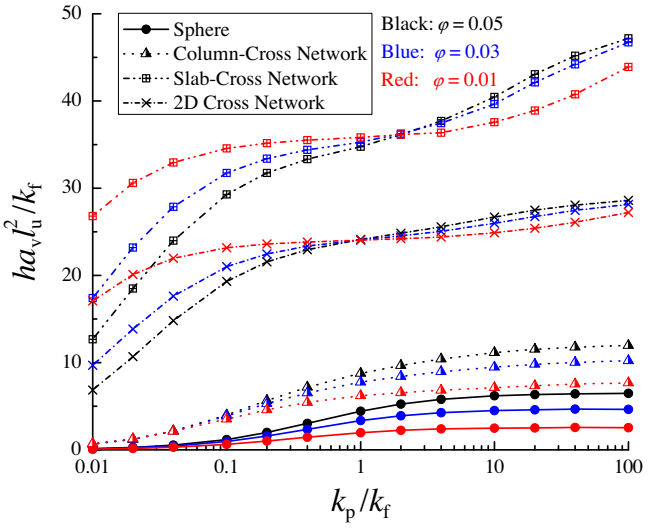

Fig. 7. Non-dimensional heat transfer coefficient $ha_v l_u^2/k_f$ as a function of particle-aggregation morphology, k_p/k_f and φ.

k_p/k_f up to $k_p/k_f = 100$. Therefore, increasing k_p/k_f value beyond a certain value is not as beneficial for nanofluids with well-dispersed nanoparticles such as the sphere nanofluids as that for nanofluids with connected particle networks in the sense of upgrading k_e/k_f.

Fig. 7 illustrates the variation of the non-dimensional heat transfer coefficient $ha_v l_u^2/k_f$ for the three nanofluids as a function of k_p/k_f and φ. The coefficient $ha_v l_u^2/k_f$ for nanofluids with the slab-cross network is much higher than those of the other two. Therefore, the enhanced particle-fluid interfacial heat transfer is the mechanism behind Hashin–Shtrikman upper conductivity bounds.

For the nanofluids containing column-cross network and sphere nanoparticles, the coefficient $ha_v l_u^2/k_f$ increases from a lower limit to a higher limit with particle-fluid conductivity ratio k_p/k_f increasing from 0 to infinity. Both limits depend on the particle shape and volume fraction. For the nanofluids containing slab-cross network, however, the simulation results do not show the two limits of $ha_v l_u^2/k_f$ at very small and very large values of k_p/k_f. Therefore, changing the particle-fluid interfacial heat transfer via varying k_p/k_f is more effective for nanofluids with the base fluid separated by the particles into the dispersed phase.

Furthermore, different particle morphologies result in different dependencies of $ha_v l_u^2/k_f$ on the particle volume fraction φ. For particle morphologies with relatively small R_g and IA, the coefficient $ha_v l_u^2/k_f$ increases with particle volume fraction over the whole range of k_p/k_f [also see Fig. 2(e)]. For the column-cross network nanofluids, the coefficient $ha_v l_u^2/k_f$ is almost the same at $\varphi = 0.05$, 0.03 and 0.01 when $k_p/k_f < 0.05$, and increases with φ when $k_p/k_f > 0.05$. For the slab-cross network nanofluids, $ha_v l_u^2/k_f$ decreases with φ when $k_p/k_f < 2$, and increases with φ when $k_p/k_f > 2$. For nanofluids containing slab-cross network, the variation trend of $ha_v l_u^2/k_f$ is similar with that for the 2D nanofluids containing connected cross networks (Fig. 7); the $ha_v l_u^2/k_f$ value is however about 50% higher than its two-dimensional counterparts [24].

The advance of volumetric interfacial heat transfer coefficient $ha_v l_u^2/k_f$ for nanofluids containing slab-cross network (SCN) compared with those containing column-cross network (CCN) could be due to either larger volumetric interfacial area a_v or enhanced volumetric heat transfer coefficient h. By using the expressions of non-dimensional interfacial area (IA) in Table 1, the a_v-ratio between SCN nanofluids and CCN nanofluids are computed to be

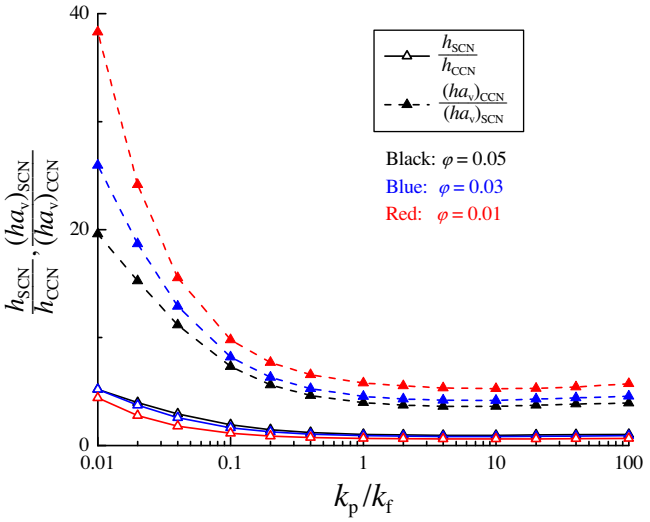

Fig. 8. h- and ha_v-ratios between slab-cross-network (SCN) nanofluids and column-cross-network (CCN) nanofluids [$(a_v)_{SCN}/(a_v)_{CCN} = 3.83,\ 4.99$ and 8.69 for $\varphi = 0.05, 0.03$ and 0.01 respectively].

3.83, 4.99 and 8.69 at $\varphi = 0.05, 0.03$ and 0.01, respectively. Accordingly, the h-ratio can be calculated by

$$\frac{h_{SCN}}{h_{CCN}} = \frac{(ha_v)_{SCN}/(ha_v)_{CCN}}{(a_v)_{SCN}/(a_v)_{CCN}} \tag{19}$$

Fig. 8 shows both $(ha_v)_{SCN}/(ha_v)_{CCN}$ and h_{SCN}/h_{CCN} as a function of k_p/k_f and φ. For all three φ values, the $(ha_v)_{SCN}/(ha_v)_{CCN}$ is always larger than one, decrease monotonously as k_p/k_f increases, and reach its asymptotic limit around $k_p/k_f = 1$. h_{SCN}/h_{CCN} also decreases monotonously as k_p/k_f increases and reach its asymptotic limit around $k_p/k_f = 1$. It is however larger than one only when k_p/k_f is smaller than 1, 0.4 and 0.1 for $\varphi = 0.05, 0.03$ and 0.01, respectively. Therefore, the higher $ha_v l_u^2/k_f$ value for SCN nanofluids comes from both enhanced h and a_v in the range of lower k_p/k_f-value and from the larger a_v only in the range of higher k_p/k_f value.

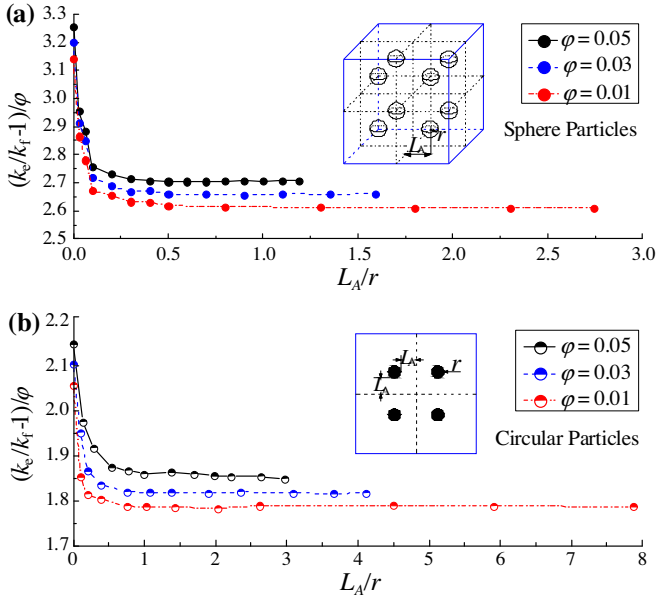

Fig. 9. Non-dimensional thermal conductivity $(k_e/k_f - 1)/\varphi$ as a function of the relative distance L_A/r, particle volume fraction φ at $k_p/k_f = 20$ (a), and a comparison with the two-dimensional nanofluids (b).

3.4. Effect of particles' aggregation

The effects of particle aggregation on the nanofluid effective thermal conductivity are examined by changing the relative separation distance between eight sphere particles defined by L_A/r as shown by the inset in Fig. 9(a). Here r and L_A are the particle radius and the distance between each particle and the center plane of unit cell respectively. When L_A/r reaches its maximum value, the nanofluids consist of uniformly-distributed sphere particles in Fig. 1(a). When $L_A/r = 0$, the eight particles touch with each other to form an aggregate; such aggregates uniformly disperse in the base fluids. Fig. 9(a) shows the variation of the non-dimensional thermal conductivity $(k_e/k_f - 1)/\varphi$ as a function of the relative distance L_A/r and particle volume fraction φ at $k_p/k_f = 20$. The $(k_e/k_f - 1)/\varphi$ decreases sharply with L_A/r when L_A/r is less than 0.2, but is nearly independent of L_A/r when L_A/r is larger than 0.2. Therefore, upgrading the nanofluid thermal conductivity via particle aggregation would be more effective and observable when the distance between particles is less than one fifth of the particle dimension. For the corresponding 2D nanofluids consisting of circular particles [24], the value of $(k_e/k_f - 1)/\varphi$ decreases sharply with L_A/r when $L_A/r < 1$, but is nearly independent of L_A/r when $L_A/r > 1$, indicating that the effect of particle aggregation on the effective thermal conductivity is observable when the distance between particles is less than the particle dimension [Fig. 9(b)].

3.5. Phase lags of heat flux (τ_q) and temperature gradient (τ_T)

For the nanofluids considered in the present work, $k_{fp}/k_f < 0.05$ [such as those shown in Figs. 2(d) and 3]. This indicates that the effect of cross-coupling between the heat conduction in the fluid and particle phases is weak. The heat conduction should thus be diffusion-dominant. To formally prove this, consider phase lags τ_T and τ_q. Both are ha_v-dependent [Eqs. (2) and (3)]. The value of ha_v can be determined from the numerical results of $ha_v l_u^2/k_f$ for given l_u which is related with the particle size through particle volume fraction φ. Taking the spherical nanoparticle with a diameter of d_p as an example, the following relation holds:

$$\frac{\frac{1}{6}\pi d_p^3}{l_u^3} = \varphi \tag{20}$$

Substituting Eqs. (8) and (20) into Eqs. (2) and (3) leads to:

$$\tau_q = \frac{1}{\frac{ha_v l_u^2}{k_f}\cdot\frac{k_f}{(\frac{\pi}{6\varphi})^{2/3}d_p^2}\left[\frac{1}{\varphi(\rho c_p)_p}+\frac{1}{(1-\varphi)(\rho c_p)_f}\right]} \tag{21}$$

$$\tau_T = \frac{(1-\varphi)(\rho c_p)_f k_{pp} + \varphi(\rho c_p)_p k_{ff}}{\frac{ha_v l_u^2}{k_f}\cdot\frac{k_f}{(\frac{\pi}{6\varphi})^{2/3}d_p^2}\cdot k_e} \tag{22}$$

Therefore, both τ_T and τ_q are proportional to d_p^2.

Consider the ratio between the two phase lags τ_T/τ_q:

$$\frac{\tau_T}{\tau_q} = 1 + \frac{\gamma_f^2 k_{pp} + \gamma_p^2 k_{ff} - 2\gamma_f\gamma_p k_{fp}}{\gamma_f\gamma_p k_e}. \tag{23}$$

It could be larger, equal or smaller than 1 depending on the sign of $\gamma_f^2 k_{pp} + \gamma_p^2 k_{ff} - 2\gamma_f\gamma_p k_{fp}$. By the condition for the existence of thermal waves that requires $\tau_T/\tau_q < 1$ [21,32], thermal waves will occur when

$$\gamma_f^2 k_{pp} + \gamma_p^2 k_{ff} - 2\gamma_f\gamma_p k_{fp} = \left(\gamma_f\sqrt{k_{pp}} - \gamma_p\sqrt{k_{ff}}\right)^2 + 2\gamma_f\gamma_p\left(\sqrt{k_{ff}k_{pp}} - k_{fp}\right) < 0. \tag{24}$$

A necessary (but not sufficient) condition for the existence of thermal waves is $k_{fp} > \sqrt{k_{ff}k_{pp}}$ which requires, by applying Eqs. (4)–(6),

$$\int_{A_{fp}} \mathbf{n}_{fp} b_l \, dA \leqslant \frac{\varphi(\varphi-1)}{k_p/k_f - \varphi(k_p/k_f - 1)} \tag{25}$$

Note that all the numerical results of k_e/k_f are bounded by Maxwell–Garnett formula [Eq. (13)] and Hashin–Shtrikman bound [Eq. (18)] for the nanofluids considered in the present work. Therefore,

$$1 + \frac{3\varphi(k_p/k_f - 1)}{k_p/k_f + 2 - \varphi(k_p/k_f - 1)} \leqslant \frac{k_e}{k_f} \leqslant \frac{k_p}{k_f}\left[1 - \frac{3(1-\varphi)(k_p/k_f - 1)}{3k_p/k_f - \varphi(k_p/k_f - 1)}\right], \quad \text{at } \frac{k_p}{k_f} > 1 \tag{26a}$$

$$\frac{k_p}{k_f}\left[1 - \frac{3(1-\varphi)(k_p/k_f - 1)}{3k_p/k_f - \varphi(k_p/k_f - 1)}\right] \leqslant \frac{k_e}{k_f} \leqslant 1 + \frac{3\varphi(k_p/k_f - 1)}{k_p/k_f + 2 - \varphi(k_p/k_f - 1)}, \quad \text{at } \frac{k_p}{k_f} < 1 \tag{26b}$$

By applying Eq. (1) and Eqs. (4)–(6), Eqs. (26a) and (26b) yield:

$$\frac{\varphi(\varphi-1)}{k_p/k_f + 2 - \varphi(k_p/k_f - 1)} \leqslant \int_{A_{fp}} \mathbf{n}_{fp} b_l \, dA \leqslant \frac{\varphi(\varphi-1)}{3k_p/k_f - \varphi(k_p/k_f - 1)}, \quad \text{at } \frac{k_p}{k_f} > 1; \tag{27a}$$

$$\frac{\varphi(\varphi-1)}{3k_p/k_f - \varphi(k_p/k_f - 1)} \leqslant \int_{A_{fp}} \mathbf{n}_{fp} b_l \, dA \leqslant \frac{\varphi(\varphi-1)}{k_p/k_f + 2 - \varphi(k_p/k_f - 1)}, \quad \text{at } \frac{k_p}{k_f} < 1. \tag{27b}$$

The right-hand-side of inequality (25), $\frac{\varphi(\varphi-1)}{k_p/k_f - \varphi(k_p/k_f-1)}$, is always negative and smaller than either $\frac{\varphi(\varphi-1)}{k_p/k_f+2-\varphi(k_p/k_f-1)}$ or $\frac{\varphi(\varphi-1)}{3k_p/k_f-\varphi(k_p/k_f-1)}$. Therefore, the inequality (25) cannot be fulfilled. The heat conduction in nanofluids with only the cross-coupling between the heat conduction in the fluid and particle phases being considered is thus diffusion-dominant. It is also interesting to note that the ratio τ_T/τ_q is independent of ha_v, and thus determined only by material properties, volume fractions and geometrical morphologies of the two phases, without influenced by the particle size.

Table 2 lists the phase lags of heat flux (τ_q) and temperature gradient (τ_T) and their ratio (τ_T/τ_q) for CuO (copper oxide)-in-water nanofluid, Al_2O_3 (alumina)-in-water nanofluid and olive-oil-in-water emulsion. For the first two types of nanofluids, the nanoparticles are assumed to be spheres with a diameter of 10 nm and connected slab-cross networks with slab thickness being 10 nm, respectively. For olive-oil-in-water emulsion, the oil phase is assumed to be spherical droplets with a diameter of 10 nm suspending in the water phase. The data in Table 2 show that τ_q and τ_T are in the order of 10^{-11} s for nanofluids with sphere nanoparticles or nanodroplets and 10^{-9}–10^{-7} s for nanofluids with connected slab-cross networks. Therefore, particle aggregation tends to increase the values of τ_q and τ_T. Moreover, τ_T/τ_q is always larger than 1 so that heat conduction in these five nanofluids is diffusion-dominant without thermal waves.

3.6. Predictive models of effective thermal conductivity

Since heat conduction is diffusion-dominant for the nanofluids considered in the present work, we can obtain some predictive models of their effective thermal conductivity by fitting our numerical results based on some classical diffusion theory in two-phase systems such as the one in [33]:

$$\frac{k_e}{k_f} = \frac{k_p/k_f + X + X\varphi(k_p/k_f - 1)}{k_p/k_f + X - \varphi(k_p/k_f - 1)} \tag{28}$$

and the classical mixture rule [34]:

$$\frac{k_e}{k_f} = \left\{1 + \varphi\left[(k_p/k_f)^n - 1\right]\right\}^{1/n} \tag{29}$$

Here X and n are the two parameters that depend on the particle shape and the conductivity ratio k_p/k_f and are listed in Table 3 for nanofluids containing spheres, cubes, hollow spheres ($r_o = 2r_i$), hollow cubes ($a_o = 2a_i$), column-cross networks and slab-cross networks. By using X and n in Table 3, the relative error for the effective thermal conductivity is less than 2% for Eq. (28) and 5% for Eq. (29). Readers are referred to [35] for a systematic review of models available for predicting the effective thermal conductivity of porous media.

Note that X equals to 2 for sphere suspensions (regardless of k_p/k_f value) and reduces to 2 when $k_p/k_f = 1$ (regardless of particle shape). This agrees well with [33] and proposes the following form of X:

$$X = \frac{k_p/k_f + a_1}{a_2 \cdot k_p/k_f + (\frac{1+a_1}{2} - a_2)} \tag{30}$$

Here a_1 and a_2 are two coefficients that depend only on the particles' morphology. Obviously, $a_1 = 0$ and $a_2 = 1/2$ for sphere nanofluid; $a_1 = a_2 = 0$ for SCN nanofluid. The existence of two independent shape coefficients is consistent with our discussion in Section 3.2 that two parameters are required to characterize the effects of particles' morphology.

In a real nanofluid the network will normally not span the whole fluid since the particles will be misoriented and randomly dispersed, especially for near-spherical particles (low R_g and IA). This partially explains the fact that the conductivity enhancement in most conventional nanofluids is much lower than the H–S upper

Table 2
Phase lags of heat flux (τ_q) and temperature gradient (τ_T), and the ratio τ_T/τ_q, for nanofluids containing sphere nanoparticles with a diameter of 10 nm or connected slabs with a thickness of 10 nm.

Nanofluids	$\varphi = 0.05$			$\varphi = 0.03$			$\varphi = 0.01$		
	$\tau_q \times 10^9$(s)	$\tau_T \times 10^9$(s)	τ_T/τ_q	$\tau_q \times 10^9$(s)	$\tau_T \times 10^9$(s)	τ_T/τ_q	$\tau_q \times 10^9$(s)	$\tau_T \times 10^9$(s)	τ_T/τ_q
CuO–H_2O (sphere)	0.0203	0.0616	3.03	0.0239	0.0754	3.15	0.0309	0.101	3.27
CuO–H_2O (slab-cross network)	2.12	28.7	13.5	3.73	63.9	17.1	12.5	290	23.2
Al_2O_3–H_2O (sphere)	0.0193	0.0614	3.18	0.0229	0.0755	3.30	0.0295	0.101	3.43
Al_2O_3–H_2O (slab-cross network)	1.97	35.6	18.1	3.43	85.9	25.0	11.4	462	40.5
Olive oil–H_2O (sphere)	0.0246	0.0411	1.67	0.0265	0.0443	1.67	0.0300	0.0499	1.66

Table 3
Parameters X and n in Eqs. (28) and (29) from the fitting of numerical results.

Particle shape	X	n
Sphere	2	$-0.31+\frac{0.98}{1+\exp\left(\frac{\ln(k_p/k_f)}{1.48}-0.64\right)}$
Cube	$\frac{k_p/k_f+0.76}{0.39k_p/k_f+0.49}$	$-0.31+\frac{0.92}{1+\exp\left(\frac{\ln(k_p/k_f)}{1.89}-0.85\right)}$
Hollow sphere	$\frac{k_p/k_f+0.36}{0.41k_p/k_f+0.26}$	$-0.30+\frac{0.86}{1+\exp\left(\frac{\ln(k_p/k_f)}{1.66}-0.98\right)}$
Hollow cube	$\frac{k_p/k_f+0.46}{0.32k_p/k_f+0.41}$	$-0.36+\frac{0.85}{1+\exp\left(\frac{\ln(k_p/k_f)}{2.07}-1.4\right)}$
Column-cross network	$\frac{k_{p/k_f+1.6}}{0.015k_p/k_f+1.285}$	$0.60-\frac{0.20}{1+\exp\left(\frac{\ln(k_p/k_f)}{0.20}+3.0\right)}$
Slab-cross network	$2k_p/k_f$	$0.90-\frac{1.64}{1+\exp\left(\frac{\ln(k_p/k_f)}{1.35}+0.67\right)}$

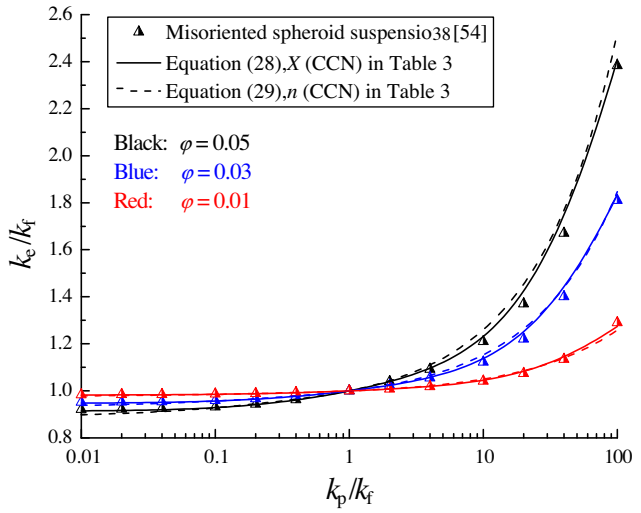

Fig. 10. Comparison between the predictive models for column-cross network nanofluid and for misoriented spheroid suspensions in [33].

bound that requires both the network spanning over the whole fluid and the base fluid being well dispersed by the network.

The effective conductivity of misoriented spheroid suspension can be predicted by [33]:

$$\frac{k_e}{k_f}=1+\frac{\varphi\beta}{1-\varphi}\frac{k_p/k_f-k_e/k_f}{k_p/k_f-1} \tag{31}$$

where

$$\beta=\frac{1}{3}\left[\frac{2}{1+(k_p/k_f-1)M/2}+\frac{1}{1+(k_p/k_f-1)(1-M)}\right]\left(\frac{k_p}{k_f}-1\right) \tag{32}$$

$$M=\frac{1}{\sin^2\phi}-\frac{1}{2}\frac{\cos^2\phi}{\sin^3\phi}\log\left(\frac{1+\sin\phi}{1-\sin\phi}\right),\quad \text{where } \cos\phi=b/a<1. \tag{33}$$

Here b/a is the spheroidal aspect ratio. With $b/a=a_c/l_u$ [Fig. 1(f) and (f′)], Fig. 10 compares the prediction from Eq. (31) with those from Eqs. (28) and (29) for CCN nanofluids (Table 3) that require the network spanning over the whole fluid only, showing a very good agreement. Therefore, our predictive models for CCN nanofluids are also capable of predicting the effective thermal conductivity for nanofluids suspended with misoriented spheroids.

4. Concluding remarks

Macroscopic heat-conduction behavior in nanofluids is characterized by their effective thermal conductivity and phase lags of heat flux and temperature gradient. The recent first-principle model links these three macroscale properties to the microscale structure of nanofluids by the closure problems. For the details of this structure–property correlation and thus a better understanding of heat conduction in nanofluids, we resolve these closure problems numerically for six typical types of nanofluids containing sphere, cube, hollow sphere, hollow cube, slab-cross and column-cross nanoparticles, respectively.

Specially, we examine numerically the effects of particle-fluid thermal conductivity ratio, particle volume fraction, and particle morphology on the effective thermal conductivity and phase lags of heat flux and temperature gradient for the six types of nanofluids. The results reveal the particle's radius of gyration and the non-dimensional particle-fluid interfacial area as the two characteristic parameters for the effect of particles' geometrical structures on the effective thermal conductivity. The nanoparticles with larger values of these two parameters can vary fluid conductivity significantly. The higher-conductivity nanofluids are always with a strong particle-fluid interfacial heat transfer. Due to the significant enhancement of this interfacial transport process, the effective thermal conductivity can practically reach the Hashin–Shtrikman bounds when particles connect to form a network and separate the base fluid into a dispersed phase. The particle aggregation will also benefit the upgrade of the effective thermal conductivity when the particles are very close to each other.

Both the phase lags of heat flux and temperature gradient are scaled with the square of particle dimension. Their values are in the range from 10^{-11} s to 10^{-7} s for the nanofluids considered in the present work. Since the phase lag of heat flux is smaller than that of temperature gradient, the heat conduction in the nanofluids examined in the present work is diffusion-dominant. Their effective thermal conductivity can be predicted adequately by the predicting models developed in the present work based on the classical diffusion theory for two-phase systems. The weak effect of cross-coupling between the heat conduction in the fluid and particle phases found in the present work does not exclude the possibility of significance of the other types of cross couplings not examined here.

Acknowledgment

The financial support from the Research Grants Council of Hong Kong (GRF718009) is gratefully acknowledged.

References

[1] U.S. Choi, Z.G. Zhang, P. Keblinski, Nanofluids, in: H.S. Nalwa (Ed.), Encyclopedia of Nanoscience and Nanotechnology, American Scientific Publishers, 2004, pp. 757–773.
[2] S.K. Das, S.U.S. Choi, W. Yu, T. Pradeep, Nanofluids: Science and Technology, John Wiley & Sons, Inc., Hoboken, New Jersey, 2008.
[3] J. Fan, L.Q. Wang, Review of heat conduction in nanofluids, ASME J. Heat Transfer 133 (2011) 040801.
[4] G.P. Peterson, C.H. Li, Heat and mass transfer in fluids with nanoparticle suspensions, Adv. Heat Transfer 39 (2006) 257–376.
[5] H.S. Chen, Y.L. Ding, Heat transfer and rheological behaviour of nanofluids: a review, in: L.Q. Wang (Ed.), Advances in Transport Phenomena, Springer-Verlag, Heidelberg, 2009.
[6] S.P. Jang, S.U.S. Choi, Role of Brownian motion in the enhanced thermal conductivity of nanofluids, Appl. Phys. Lett. 84 (21) (2004) 4316–4318.
[7] R. Prasher, P. Bhattacharya, P.E. Phelan, Thermal conductivity of nanoscale colloidal solutions (nanofluids), Phys. Rev. Lett. 94 (2) (2005) 025901.
[8] X. Wang, X. Xu, S.U.S. Choi, Thermal conductivity of nanoparticle-fluid mixture, J. Thermophys. Heat Transfer 13 (1999) 474–480.

[9] S.U.S. Choi, Z.G. Zhang, W. Yu, F.E. Lockwood, E.A. Grulke, Anomalous thermal conductivity enhancement in nanotube suspensions, Appl. Phys. Lett. 79 (14) (2001) 2252–2254.
[10] P. Keblinski, S.R. Phillpot, S.U.S. Choi, J.A. Eastman, Mechanisms of heat flow in suspensions of nano-sized particles (nanofluids), Int. J. Heat Mass Transfer 45 (2002) 855–863.
[11] W. Evans, R. Prasher, J. Fish, P. Meakin, P. Phelan, P. Keblinski, Effect of aggregation and interfacial thermal resistance on thermal conductivity of nanocomposites and colloidal nanofluids, Int. J. Heat Mass Transfer 51 (2008) 1431–1438.
[12] P.E. Gharagozloo, J.K. Eaton, K.E. Goodson, Diffusion, aggregation, and the thermal conductivity of nanofluids, Appl. Phys. Lett. 93 (10) (2008) 103110.
[13] P.E. Gharagozloo, K.E. Goodson, Aggregate fractal dimensions and thermal conduction in nanofluids, J. Appl. Phys. 108 (7) (2010) 074309.
[14] P.E. Gharagozloo, K.E. Goodson, Temperature-dependent aggregation and diffusion in nanofluids, Int. J. Heat Mass Transfer 54 (2011) 797–806.
[15] W. Jiang, L.Q. Wang, Monodisperse magnetite nanofluids: Synthesis, aggregation, and thermal conductivity, J. Appl. Phys. 108 (11) (2010) 114311.
[16] J. Philip, P.D. Shima, B. Raj, Evidence for enhanced thermal conduction through percolating structures in nanofluids, Nanotechnology 19 (2008) 305706.
[17] J. Philip, P.D. Shima, B. Raj, Nanofluid with tunable thermal properties, Appl. Phys. Lett. 92 (4) (2008) 043108.
[18] R. Prasher, P.E. Phelan, P. Bhattacharya, Effect of aggregation kinetics on the thermal conductivity of nanoscale colloidal solutions (Nanofluids), Nano Lett. 6 (7) (2006) 1529–1534.
[19] L.Q. Wang, J. Fan, Toward nanofluids of ultra-high thermal conductivity, Nanoscale Res. Lett. 6 (2011) 153.
[20] L.Q. Wang, M. Quintard, Nanofluids of the future, in: L.Q. Wang (Ed.), Springer, New York, 2009, pp. 179–248.
[21] L.Q. Wang, X.S. Zhou, X.H. Wei, Heat Conduction: Mathematical Models and Analytical Solutions, Springer-Verlag, Berlin, Heidelberg, 2008.
[22] J. Buongiorno, D.C. Venerus, N. Prabhat, T. McKrell, J. Townsend, R. Christianson, Y.V. Tolmachev, P. Keblinski, L.W. Hu, J.L. Alvarado, I.C. Bang, S.W. Bishnoi, M. Bonetti, F. Botz, A. Cecere, Y. Chang, G. Chen, H.S. Chen, S.J. Chung, M.K. Chyu, S.K. Das, R. Di Paola, Y.L. Ding, F. Dubois, G. Dzido, J. Eapen, W. Escher, D. Funfschilling, Q. Galand, J.W. Gao, P.E. Gharagozloo, K.E. Goodson, J.G. Gutierrez, H.P. Hong, M. Horton, K.S. Hwang, C.S. Iorio, S.P. Jang, A.B. Jarzebski, Y.R. Jiang, L.W. Jin, S. Kabelac, A. Kamath, M.A. Kedzierski, L.G. Kieng, C. Kim, J.H. Kim, S. Kim, S.H. Lee, K.C. Leong, I. Manna, B. Michel, R. Ni, H.E. Patel, J. Philip, D. Poulikakos, C. Reynaud, R. Savino, P.K. Singh, P.X. Song, T. Sundararajan, E. Timofeeva, T. Tritcak, A.N. Turanov, S. Van Vaerenbergh, D.S. Wen, S. Witharana, C. Yang, W.H. Yeh, X.Z. Zhao, S.Q. Zhou, A benchmark study on the thermal conductivity of nanofluids, J. Appl. Phys. 106 (9) (2009) 094312.
[23] J. Eapen, R. Rusconi, R. Piazza, S. Yip, The classical nature of thermal conduction in nanofluids, ASME J. Heat Transfer 132 (2010) 102402.
[24] J. Fan, L.Q. Wang, Effective thermal conductivity of nanofluids: the effects of microstructure, J. Phys. D: Appl. Phys. 43 (16) (2010) 165501.
[25] Z. Hashin, S. Shtrikman, A variational approach to the theory of the effective magnetic permeability of multiphase materials, J. Appl. Phys. 33 (10) (1962) 3125–3131.
[26] L.Q. Wang, X.H. Wei, Heat conduction in nanofluids, in: K. Sattler (Ed.), Handbook of Nanophysics, Taylor & Francis, 2010, pp. 33.31–33.35.
[27] M. Quintard, S. Whitaker, One- and two-equation models for transient diffusion processes in two-phase systems, Adv. Heat Transfer 23 (1993) 369–464.
[28] L.Q. Wang, K.C. Cheng, Flow transitions and combined free and forced convective heat transfer in rotating curved channels: the case of positive rotation, Phys. Fluids 6 (1996) 1553–1573.
[29] L.Q. Wang, T.L. Yang, Multiplicity and stability of convection in curved ducts: reviews and progress, Adv. Heat Transfer 38 (2004) 203–255.
[30] J.C. Maxwell, Treatise on Electricity and Magnetism, Clarendon Press, Oxford, 1873.
[31] J. Fan, L.Q. Wang, Microstructural effects on macroscale thermal properties in nanofluids, NANO 5 (2) (2010) 117–225.
[32] D.Y. Tzou, Macro- to Microscale Heat Transfer: The Lagging Behavior, Taylor & Francis, Washington, DC, 1997.
[33] H. Fricke, A mathematical treatment of the electric conductivity and capacity of disperse systems: I. The electric conductivity of a suspension of homogeneous spheroids, Phys. Rev. 24 (1924) 575–587.
[34] L.E. Nielsen, Predicting the Properties of Mixtures: Mixture Rules in Science and Engineering, Marcel Dekker, New York, 1978.
[35] P. Cheng, C.T. Hsu, The effective stagnant thermal conductivity of porous media with periodic structures, J. Porous Media 2 (1999) 19–38.